Article:
Guo, J, Zhu, H, Xu, H et al. (2 more authors) (2020) Spinnable mesophase pitch prepared via co-carbonization of fluid catalytic cracking decant oil and synthetic naphthalene pitch. Energy & Fuels, 34 (2). pp. 2566-2573. ISSN 0887-0624

https://doi.org/10.1021/acs.energyfuels.9b03841

Spinnable mesophase pitch prepared via co-carbonization of fluid catalytic cracking decant oil and synthetic naphthalene pitch

Jianguang Guo[a,b], Hui Zhu[c], Huitao Xu[a,b], Aidan Westwood[d] , Xuanke Li[a,b,c]*

[a] College of Materials Science and Engineering, Hunan University, Yuelu Mountain, Changsha 410082, China

[b] Hunan Province Key Laboratory for Advanced Carbon Materials and Applied Technology, Hunan University, Changsha 410082, China

[c] The State Key Laboratory of Refractories and Metallurgy, Wuhan University of Science and Technology, Wuhan 430081, China

[d] School of Chemical and Process Engineering, University of Leeds, Leeds, LS2 9JT, United Kingdom

Abstract：Using, as starting materials, fluid catalytic cracking decant oil (FDO), rich in short-chain alkyl groups, and synthetic naphthalene pitch (NP), with stable naphthenic structures, the synthesis of a spinnable mesophase pitch via a co-carbonization process was investigated. The effects of NP addition and the precursor molecular structure on properties of the resultant mesophase pitches and their carbon fiber derivatives were also discussed. With the increase of NP inclusion from 10wt% to 30wt%, the solubility in Toluene and Quinoline and the optically anisotropic domain size of the synthesized pitches increase. However, the softening points of the resultant mesophase pitches decrease. In comparison with FDO, more naphthenic structures are retained in NP and these show higher thermal stability during the preparation of mesophase pitch. The interaction of naphthenic structures in NP and short-chain alkyl groups in FDO promotes an increase in the molecular weight of the mesophase pitch prepared via co-

carbonization and, in the present case, also increases the orientation and domain size in the resulting mesophase liquid crystal. The synthesized mesophase possesses low softening point, good solubility and 100 vol% mesophase content. Carbon fibers prepared from the co-carbonized mesophase pitch exhibit higher thermal conductivity than that of K-1100.

Key words : Spinnable mesophase pitch, co-carbonization, fluid catalytic cracking decant oil, naphthenic structures, interactive effect.

1. Introduction

Spinnable mesophase pitch has been commonly recognized as an excellent intermediate for pitch-based carbon fiber with high performance due to its highly oriented molecular alignment, high coking value and low viscosity [1-2]. Petroleum byproducts with abundant aromatic fractions have been extensively used to produce high-quality mesophase pitch because of their low cost [3-4]. Therefore, using petroleum byproduct as feedstock to prepare mesophase pitch is a focus of activity in the field of carbon materials.

As a byproduct of catalytic cracking of heavy crude oil, fluid catalytic cracking decant oil (FDO), which contains a high content of polycyclic aromatic hydrocarbon, can be used for preparation of mesophase pitch [5]. However, it is difficult to control the molecular structure and optical texture of the mesophase pitch derived from FDO via single thermal treatment because of its wide molecular weight distribution and, especially, because of the highly decomposed active components of the raw material [6]. As a result, such mesophase pitches usually exhibit high softening point and low solubility. In order

to avoid these problems, several additional steps such as hydrotreatment [7-8], extensive removal of volatile components [9-10] and extraction of non-fusible components [11-12] have been used to prepare high quality mesophase pitch. However, this inevitably decreases the yield and raises the process complexity and cost of the mesophase pitch.

There is a consensus that some favorable properties of the mesophase pitch, such as low softening point, high solubility and optical texture are ascribed to their naphthenic structures and moderate length aliphatic groups in their precursor pitches [13-14]. On the other hand, pure aromatic hydrocarbons have proven to be excellent precursors for preparing spinnable mesophase pitch by catalytic synthesis [15-17]. The synthetic pitch prepared from naphthalene contains a large amount of naphthenic hydrogens, which reduce its softening point and enhance the solubility of the resultant mesophase pitch [17].

To improve the poor attributes of mesophase pitch prepared from FDO feedstock whilst avoiding the abovementioned problems of process complexity, synthetic naphthalene pitch (NP, with abundant naphthenic structures) has been therefore selected in this work for co-carbonization with FDO in order to prepare spinnable mesophase pitch. The effects of NP addition and the precursor molecular structures (particularly the naphthenic structures) on properties of the mesophase pitch products and their carbon fiber derivatives are investigated. The interaction of the two feedstocks during the formation of mesophase pitch is also elucidated.

2. Experimental

2.1 The preparation of mesophase pitch and its carbon fiber derivatives

Fluid catalytic cracking decant oil (FDO) was provided by Jinzhou Petrochemical Co., China. Using HF/BF_3 as catalyst and naphthalene as starting material, the synthetic naphthalene pitch (NP) was prepared by catalytic polymerization in an autoclave at 90 °C under 0.4-0.5 MPa autogenous pressure for 3h [17]. The general properties of the two feedstocks are summarized in Table 1. Notably, FDO's much lower carbon residue content indicated that it contains a large number of labile components.

Table 1 General properties of the two feedstocks

Sample	SP[a] /°C	TS[b]/%	Elemental analysis/wt.%				n(H)/n(C)	CR[c]/%
			C	H	N	S		
FDO	---	98.9	90.640	9.043	0.380	0.270	1.197	7.30
NP	93	95.2	93.861	6.102	0.001	0.018	0.780	61.97

[a] Softening point, [b] Toluene soluble, [c] Carbon residue content at 600°C, evaluated by TGA

FDO and NP were mixed in mass ratios of 100:0, 90:10, 80:20, 70:30 and 0:100 to form the basic feedstocks, which were labelled as FDO-NP (0), FDO-NP (10), FDO-NP (20), FDO-NP (30) and FDO-NP (100), respectively. These mixtures of FDO and NP (ca.40-50 g) were co-carbonized at 420 °C for 6 h under a reaction pressure of 4~6 MPa in a 100ml autoclave. The naphthalene pitch powder and the FDO were mixed homogeneously by stirring for 30 min before loading into the autoclave to fully dissolve the naphthalene pitch in the FDO and they were then homogeneously blended by nitrogen bubbling. The products were then heated in a quartz tube (diameter of 25 mm and length of 180 mm) placed in a vertical electric furnace at 400 °C for 10 h under a nitrogen flow of 300 ml/min. The nitrogen

bubbling prevented the sample from oxidization and blended the sample homogeneously during the reaction. After this heat treatment, the quartz tube was rapidly cooled in air to fix the anisotropy in the resultant pitches and then the quartz tube was broken carefully to remove the resultant pitches. The mesophase pitches prepared from the above mixtures were labelled as FDO-NP(0)-MP, FDO-NP(10)-MP, FDO-NP(20)-MP, FDO-NP(30)-MP and FDO-NP(100)-MP, respectively. The heating rate of the co-carbonization and thermal polymerization processes was ~5 °C /min in all cases.

The mesophase pitch FDO-NP(20)-MP was selected for melt-spinning through a circular shaped spinning nozzle (diameter = 0.2 mm, length over diameter (L/D) = 3) under nitrogen pressure of 0.2 MPa. Melt-spinning was conducted at 330 °C at a winding speed of 400 m/min. The as-spun mesophase pitch fiber was then oxidatively stabilized in air at 280 °C for 0.5 h with a heating rate of 0.5 °C /min. The stabilized fiber, with a weight gain of 10.2 wt.%, was carbonized at 1000 °C for 30 min following a heating rate of 5 °C /min and then the resulting carbon fiber was further graphitized at 3000 °C for 10 min.

2.2 Characterization

A capillary rheometer (CFT-100EX, Shimadzu) was used to determine the softening points of raw materials and mesophase pitches. The carbon, hydrogen, nitrogen and sulfur contents of the samples were determined using an elemental analyzer (Elementar Vario EL III). The Fourier transform infrared (FTIR) spectra of samples were determined using KBr pellets of solid samples in a Thermo Fisher IS10 FTIR spectrometer (Thermo Fisher). To elucidate the structures of the feedstocks and the prepared mesophase pitches, ^{1}H NMR and ^{13}C NMR analyses were performed using a Bruker Avance DMX-500

spectrometer with deuterated pyridine (C_5D_5N) and tetramethylsilane (TMS) as solvent and internal standard, respectively [18]. The molecular weight distributions of raw materials and mesophase pitches were evaluated by matrix-assisted laser desorption/ionization time of flight (MALDI TOF) mass spectrometer (Bruker Daltonics), without matrix-assist [19], and tetrahydrofuran (THF) was used as solvent. The fine powder sample was dissolved in THF (0.5% w/v) and 0.5 μL of the dissolved sample (including soluble components and insoluble components dispersed in the solvent) was loaded on the target cell and air-dried. The operating parameters were adjusted to a laser beam attenuation of 66%, delay time of 120 ns and laser repetition rate of 100 Hz (without matrix-assist). The optical microstructures of the mesophase pitches were analyzed by using an Olympus BX53M polarized light microscope (PLM) and the polarized light photomicrographs were then processed by the irregular shape area calculation function of Image Pro Plus Software for evaluation of the anisotropic content. According to the report by Eser [20], the anisotropic microstructures were divided into four types: (1) mosaic (M; feature size < 10 μm); (2) small domain (SM; feature size of 10−60 μm); (3) domain (D; feature size > 10 μm); (4) large domain (LD; length size > 60 μm, width > 10 μm).

The molecular stacking and orientation of the mesophase pitches as well as the crystal structure of mesophase pitch-based carbon fibers were characterized by wide-angle X-ray diffraction (XRD, D8, Bruker) with Cu Kα radiation (λ=0.15406 nm). The *d*-spacing and the average stacking height (L_c) of the (002) planes of the graphitic crystal were calculated using the Bragg equation [21] and Scherrer's equation [22], respectively.

The average axial electrical resistivities of the fibers were calculated from measurements of fifteen individual graphitized fibers using a standard four-probe method. The mechanical properties of the carbon fibers were measured using a single-filament testing machine according to ASTM standard D3822-14. The transverse cross-sectional area of each broken carbon fiber end was measured and calculated using a scanning electron microscope (SEM, JFM-6700F, JEOL).

3. Results and discussion

3.1 Molecular structure analysis of FDO and NP

Fig. 1 illustrates the FT-IR spectra of the two feedstocks. Compared to that of FDO, the FT-IR spectrum of NP shows stronger peaks at 3040, 1600 and 880-750 cm^{-1} corresponding to aromatic C-H and C=C stretching vibrations as well as aromatic out-of-plane C-H bending, respectively, owing to NP's higher aromaticity. The stronger alkyl C-H stretching vibration peak at 2920-2860 cm^{-1} and methylene C-H bending vibration peak at 1450 cm^{-1} (including methylene in naphthenic structures) of the FT-IR spectrum for FDO suggest an abundance of alkyl groups in FDO. What is noteworthy is that a much stronger peak, at 1380 cm^{-1}, can be attributed to methyl C-H bending vibration in FDO. This indicates that there is a greater abundance of methyl groups in FDO than in NP.

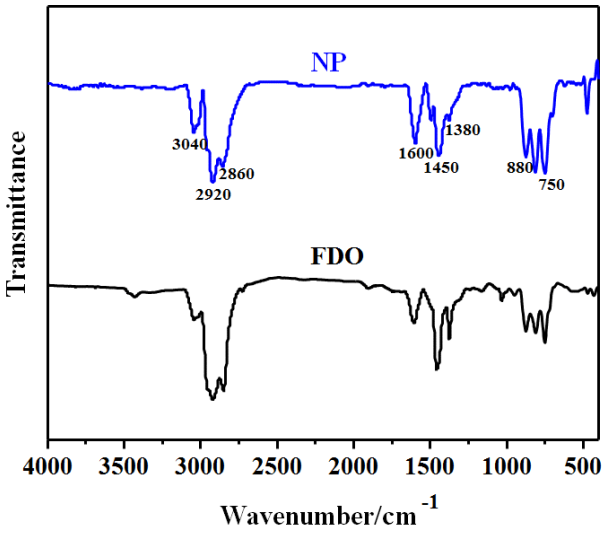

Fig.1. FT-IR spectra of the FDO and NP

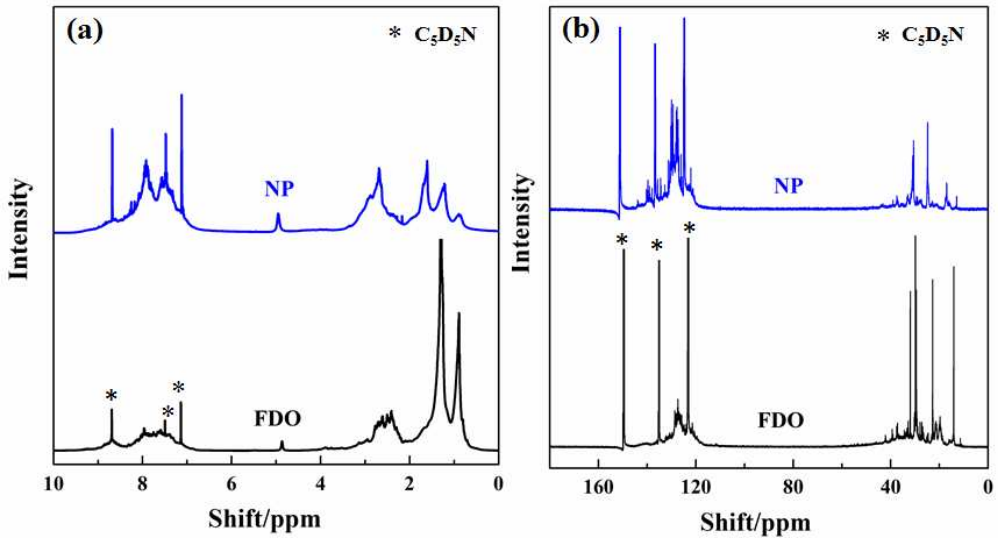

Fig. 2. ^{1}H-NMR (a) and ^{13}C-NMR (b) spectra of FDO and NP

Fig. 2 shows ^{1}H-NMR and ^{13}C-NMR spectra of FDO and NP. The solvent peaks' integral areas were obtained from the spectrogram by MestReNova software. After deducting the solvent peaks' areas, the quantitative hydrogen and carbon distributions obtained by integrating the NMR spectrum are summarized in Table 2 and Table 3, respectively. ^{1}H-NMR analyses reveal that FDO and NP have

naphthenic hydrogen abundances up to 32.7% and 17.6%, respectively. ^{13}C-NMR analyses show that the FDO contains methyl group abundances up to 12.9% compared to the 3.8% of NP. The much higher aromaticity of NP (fa=0.71) results from its higher polyaromatic content. Overall, FDO contains abundant naphthenic structures and short alkyl chains while NP is rich in naphthenic structures but has only a few short alkyl chains.

Table 2 Hydrogen distributions in FDO and NP [23].

Sample	H_{aro}/%	H_F/%	H_α/%	H_β/%	H_γ/%	H_n/%
FDO	18.9	1.3	21.9	44.8	14.4	32.7
NP	46.8	2.6	29.7	19.7	3.8	17.6

H_{aro}: Aromatic hydrogen (10.0-6.0 ppm).

H_F: Aliphatic hydrogen in methylene groups to two aromatic rings (4.5-3.3 ppm).

H_α: Aliphatic hydrogen in methyl or methylene groups in α-position to an aromatic ring (4.5-2.0 ppm).

H_β: Aliphatic hydrogen in methyl or methylene groups in β-position to an aromatic ring (2.0-1.1ppm).

H_γ: Aliphatic hydrogen in methyl or methylene groups in γ-position to an aromatic ring (1.1-0.3 ppm).

H_n: Naphthenic hydrogen (2.0-1.4 ppm).

Table 3 Carbon distributions in FDO and NP [24].

Sample	Aromatic/%		Aliphatic/%			fa
	$C_{ar1,2}$	$C_{ar1,3}$	$C_{\alpha 2}$	CH_2	CH_3	
FDO	10.6	32.6	16.0	27.9	12.9	0.43
NP	30.9	40.2	6.9	18.2	3.8	0.71

$C_{ar1,2}$: Catacondensed aromatic carbons, aromatic carbon with heteroatomic or aromatic substituents, aromatic carbons joined to aliphatic chains (160.1-129.5 ppm).

$C_{ar1,3}$: Pericondensed or protonated aromatic carbons (129.5-108 ppm).

$C_{\alpha 2}$: Bridge/hydroaromatic structures (49.3-34 ppm).

CH_2: All other methylene carbons (34-23 ppm).

CH_3: Aliphatic carbon of methyl groups (23-17 ppm).

Fig. 3 shows TOF-mass spectra of FDO and NP. The average molecular weight (M_n) has been evaluated by relating the intensity of the mass spectrum [25]. Fig. 3 shows that molecular weight peak distributions of FDO and NP are multimodal and the main molecular weight concentrations of both FDO and NP are at m/z = 250-800 and 250-1000, respectively. The average molecular weight of the FDO and NP were m/z = 423 and m/z = 600, respectively.

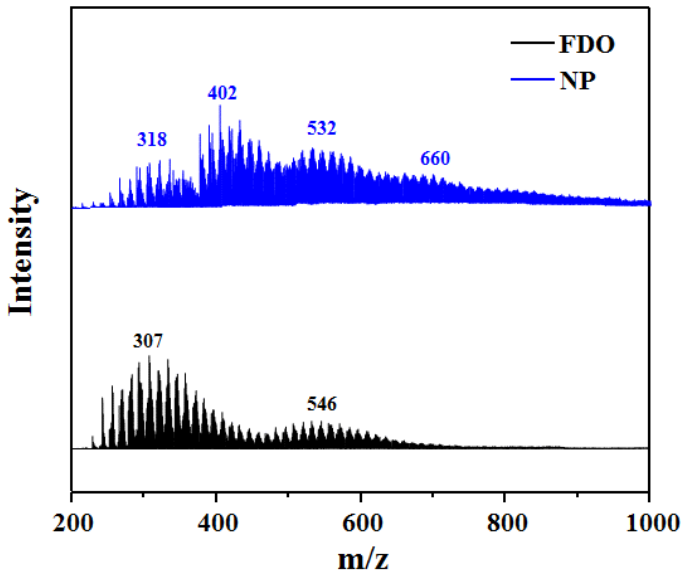

Fig. 3. TOF-MS spectra of the FDO and NP

In order to understand the differences in molecular structure between the above two feedstocks, hypothetical molecular models of FDO and NP based on the ^{1}H-NMR, ^{13}C-NMR and TOF-MS data are suggested as shown in Fig. 4. The hypothetical molecular model of FDO shown in Fig. 4(a), consists of a four-ring aromatic plane with abundant short alkyl chains (-CH_3) and a large number of naphthenic structures. In comparison with FDO, the hypothetical molecular model of the NP shown in Fig. 4(b) contains only a few short alkyl chains (-CH_3) and is rich in naphthenic structures within a larger aromatic plane.

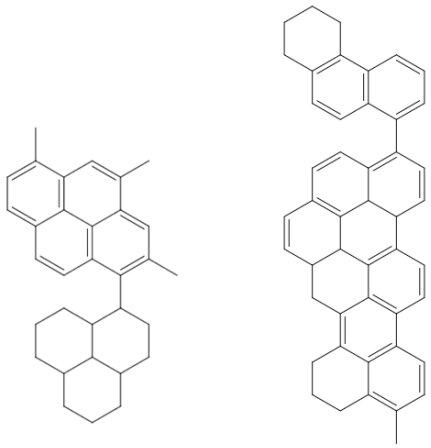

Fig. 4. Hypothetical molecular models of the feedstocks: (a) FDO and (b) NP

3.2 General properties and optical texture of mesophase pitches derived from co-carbonization

General properties of the resultant mesophase pitches are summarized in Table 4. All the mesophase pitches exhibit almost 100 vol% anisotropy under PLM, except that the FDO-NP(0)-MP shows an anisotropy content near to 85 vol%. This lower anisotropic content implies that FDO derived mesophase pitch might possess lower molecular weight components. The initial mesophase spheres were generated uniformly, and then the mesophase pitches, possessing large domain structure, narrow molecular weight distribution and similar molecular structure character to their feedstocks, were produced [26]. The formation of the resultant mesophase pitches with large optical texture by a co-carbonization process may result from the closed average molecular weight distributions of FDO and NP as revealed by the TOF-MS spectra. As shown in Table 4, with the increase of NP content from 0% to 30%, the softening points (SP) of the corresponding mesophase pitches decrease significantly from 315 °C to 266 °C and their quinoline insoluble (QI) contents decrease from 47.5% to 27.8% to the accompaniment of a slight

increase in their H/C molar ratios. This indicates that the mobility and solubility of the synthesized mesophase pitches are obviously improved owing to the introduction of NP. The yield of mesophase pitches prepared by co-carbonization is higher than the calculated yield (CY) based on the mesophase pitch yield of individual FDO and NP and their mass ratios in the mixed raw materials, as shown in Table 4. This suggests an interaction rather than a simple mixture effect between FDO and NP during the co-carbonization process [6]. The CY value of the mesophase pitch FDO-NP(X)-MP was calculated by the formula: CY%=20.0*(100-X) + 50.2*X, where X is the NP content in the raw materials.

Table 4 Some general properties of mesophase pitches from FDO-NP co-carbonization

Sample	Yield/%	CY/%	SP[θ]/°C	AC[d]/%	TS[e]/%	QI[f]/%	n(H)/n(C)
FDO-NP(0)-MP	20.0	20.0	315	80~85	18.4	47.5	0.546
FDO-NP(10)-MP	25.3	23.0	290	95~98	31.3	39.3	0.565
FDO-NP(20)-MP	29.2	26.0	275	100	35.4	34.6	0.566
FDO-NP(30)-MP	34.5	29.1	266	100	36.4	27.8	0.569
FDO-NP(100)-MP	50.2	50.2	260	100	42.9	23.5	0.563

[θ] The SP of commercial AR mesophase pitch measured by the same method is 267 °C and the SP of commercial AR mesophase pitch measured by Mettler method is 297 °C, [d] Anisotropic content, [e] Toluene soluble, [f] Quinoline insoluble.

The anisotropic component content and the optical texture of mesophase pitch are key factors that influence its subsequent melt-spinning performance. Fig. 5 shows the optical micrographs of these mesophase pitches. It can be seen from Fig. 5 that the optically anisotropic area and content of the

mesophase pitch developed with the increase of NP content in the precursor. FDO-NP(0)-MP shown in Fig. 5(a) shows medium size anisotropic texture and a certain amount of island-like isotropic domains. Excessive free radicals formed by FDO pyrolysis result in the rapid increase of system viscosity which promotes the formation of low anisotropic content and small anisotropic domains [27]. With the increase of NP to 10wt%, large anisotropic domains with only very small areas of isotropic spheres between them are observed (shown in Fig. 5(b)). With further increase of NP to 20 and 30wt%, FDO-NP(20)-MP and FDO-NP(30)-MP were produced with 100 vol% anisotropic mesophase content as shown in Fig. 5(c) and (d), respectively. This suggests that they may have better rheological properties and ordered optical texture for melt-spinning. The co-carbonization both NP and FDO appears to promote the development and coalescence of liquid crystal phase structure in the resultant mesophase pitches owing to the introduction of naphthenic structures. Hydrogen transfer reactions in the naphthenic structures may moderate the production of free radicals, thereby giving the aromatic molecules enough time to coalesce and be arranged in orderly structures [18].

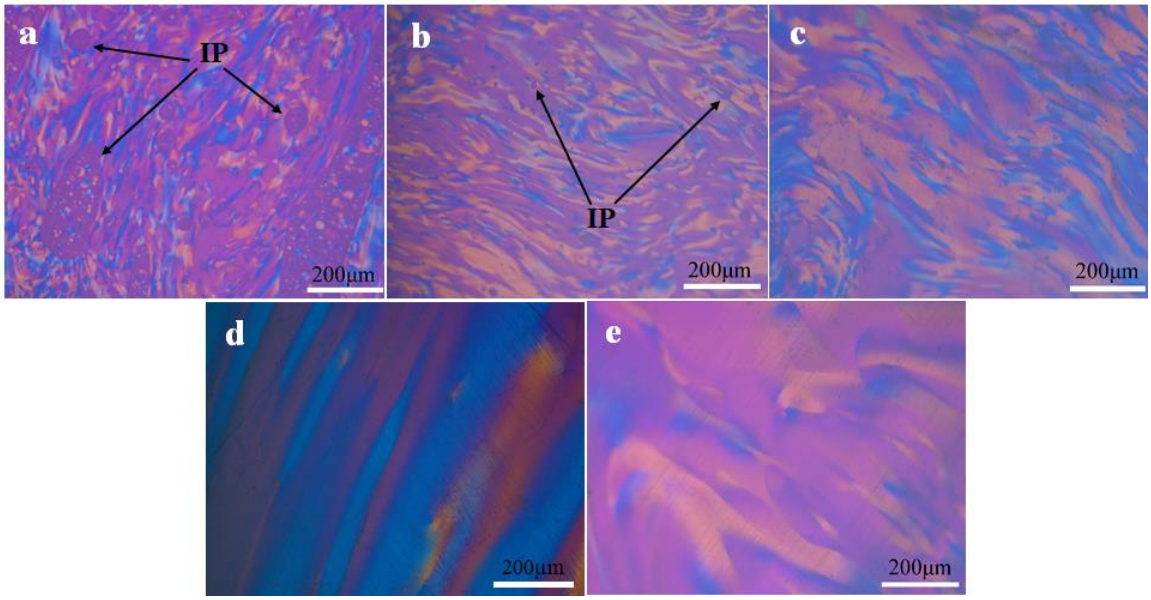

Fig. 5. Optical micrographs of the mesophase pitches: (a) FDO-NP(0)-MP, (b) FDO-NP(10)-MP, (c) FDO-NP(20)-MP, (d) FDO-NP(30)-MP and (e) FDO-NP(100)-MP.

3.3 Molecular and crystal structures of mesophase pitches

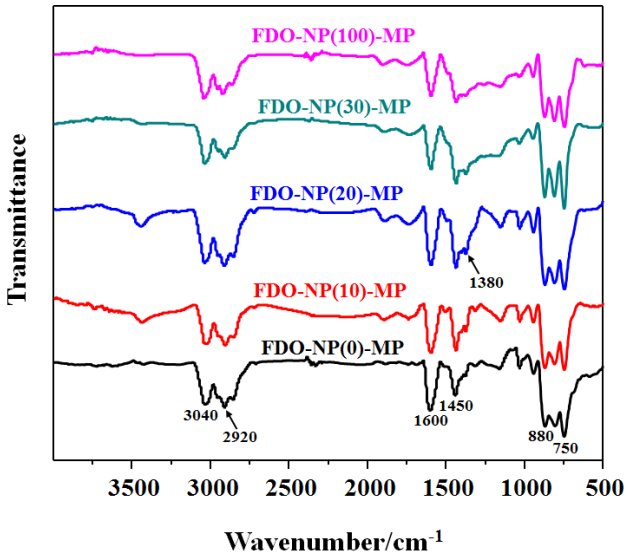

Fig. 6. FT-IR spectra of the mesophase pitches.

Fig. 6 shows the FT-IR spectra of the mesophase pitch products. It can be observed that the intensities of the IR absorption peak at 2920-2860 and 1450 cm^{-1} decrease with the increase of NP in the corresponding feedstock, suggesting that the aliphatic content in the resulting mesophase pitches also decreases. In order to quantitatively analyze the molecular structure of the synthesized mesophase pitches, the peak intensity ratio of (i) isolated aromatic C-H to (ii) aromatic C=C, related to the degree of cata-condensation of polycyclic aromatic hydrocarbons (PAH), was denoted as Abs_{880}/Abs_{1600}. The aromatic index (I_{ar}) of mesophase pitch was also defined as the formula: $Abs_{3040}/(Abs_{3040} + Abs_{2920})$ [28], and the molar ratios of $-CH_2-$ to $-CH_3$ (R) were calculated using the formula

R=3.07Abs_{1450}/Abs_{1380}-3.72. The ortho-substitution index (I_{os}), representing the relative size of aromatic molecules, was calculated using the formula I_{os}=Abs_{750}/(Abs_{750} + Abs_{815} + Abs_{880}) [28]. The terms Abs_{2920}, Abs_{1380}, Abs_{1450} and Abs_{1600} represented the absorption peak areas determined by deconvolution of the peaks at 2920, 1380, 1450 and 1600 cm^{-1}, respectively [29]. The calculated parameters are summarized in Table 5.

Table 5 Calculated parameters based on FTIR spectra of mesophase pitches

Sample	I_{ar}	I_{os}	R	Abs_{880}/Abs_{1600}
FDO-NP(0)-MP	0.752	0.369	1.220	1.577
FDO-NP(10)-MP	0.761	0.384	1.337	1.613
FDO-NP(20)-MP	0.803	0.411	1.650	1.721
FDO-NP(30)-MP	0.826	0.457	1.913	1.776
FDO-NP(100)-MP	0.852	0.385	2.136	1.932

Table 5 shows that both Abs_{880} /Abs_{1600} and aromatic index (I_{ar}) of the prepared mesophase pitches increase with NP weight ratio in the feedstocks. The table also implies that the aliphatic content in the mesophase pitches decreases with increasing NP content in the feedstocks. The same tendency in the molar ratios of -CH_2- to -CH_3 (R) suggests that methylene group content (including methylene groups in naphthenic structures) in the resultant mesophase pitches increases with weight ratio of NP in the feedstocks. The ortho-substitution index (I_{os}) of the mesophase pitches prepared via co-carbonization are higher than that of individual FDO or NP based mesophase pitch (except for FDO-NP(10)-MP vs FDO-NP(100)-MP), suggesting that the mesophase pitches prepared by co-carbonization possess

relatively larger molecular sizes. This behavior might be explained by synergistic reaction of FDO and NP during the co-carbonization. The abundant naphthenic structures in NP and short-chain alkyl groups (especially methyl groups) in FDO could contribute to maintaining good fluidity of the reaction system, which is considered to be beneficial for the polymerization of aromatic molecules [18].

Fig. 7(a) shows the ^{1}H-NMR spectra of the pyridine-soluble components of the mesophase pitch products and the hydrogen distributions after the solvent peaks were deducted are summarized in Table 6.

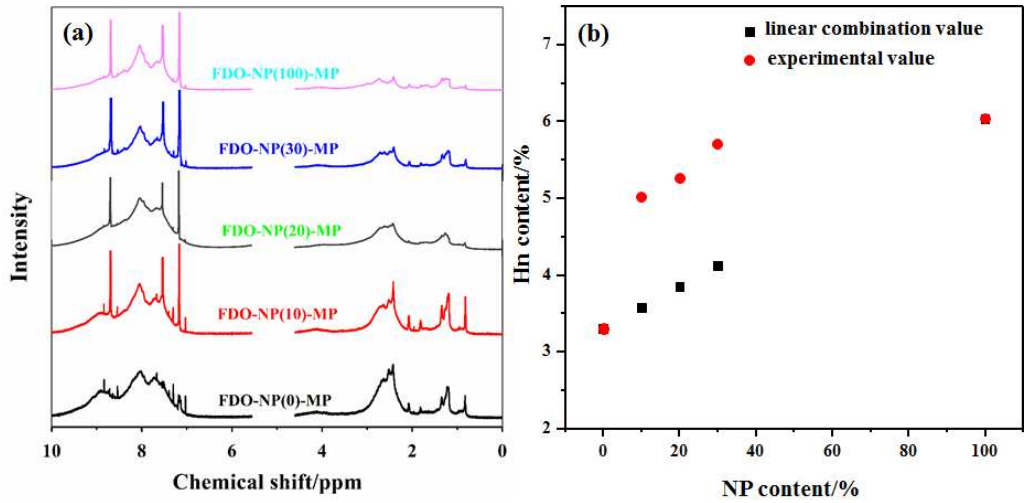

Fig. 7. (a) ^{1}H-NMR spectra and (b) Hn content of pyridine-soluble components of the mesophase pitches

As shown in Table 6, the aromaticity index of the mesophase pitches increases from 0.884 to 0.920 with increasing NP weight ratio in their feedstocks. The H_{β} and H_{γ} contents are much smaller than H_{α} and do not show significant change with the addition of NP, suggesting that the aliphatic structures in the mesophase pitch products are mainly short alkyl chains. In addition, FDO-NP(0)-MP and FDO-

NP(100)-MP possesses the lowest and the highest H_n percent of 3.30% of 6.04%, respectively. Although FDO and NP possesses naphthenic structures of 32.7% and 17.6%, respectively, as shown in Table 2. This suggests that the naphthenic structures of the feedstocks partly remained in their mesophase pitch products after the polymerization [30] and the naphthenic structures in NP obviously shown higher thermal stability than that in FDO. Additionally, the $\%H_n$ value for mesophase pitches prepared via co-carbonization increases with NP weight ratio in the feedstock, and the experimentally measured H_n hydrogen content is higher than the expected linear combination value from FDO-NP(0)-MP and FDO-NP(100)-MP (calculated based on the H_n hydrogen content of individual FDO-NP(0)-MP and FDO-NP(100)-MP according to their mass ratios) as shown in Fig. 7(b)). This indicates that more naphthenic structures than expected from the raw materials were preserved in the mesophase pitch products owing to a synergistic reaction such as hydrogen transfer or naphthenic transfer reactions during the co-carbonization process [13,23].

Table 6 Hydrogen distributions of the resultant mesophase pitches

Sample	H_{aro}/%	H_F/%	H_α/%	H_β/%	H_γ/%	H_n/%	fa
FDO-NP(0)-MP	57.62	4.30	31.79	8.94	1.65	3.30	0.884
FDO-NP(10)-MP	59.18	3.93	29.21	9.24	2.37	5.02	0.885
FDO-NP(20)-MP	63.40	3.71	26.81	8.62	1.17	5.26	0.896
FDO-NP(30)-MP	65.78	3.65	23.59	9.30	1.33	5.71	0.902
FDO-NP(100)-MP	71.27	3.10	18.59	9.01	1.13	6.04	0.920

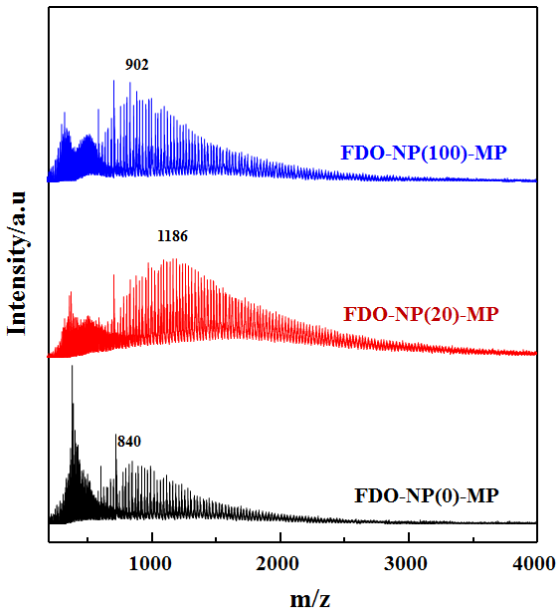

Fig. 8. TOF-MS spectra of selected mesophase pitches

Fig. 8 shows the TOF-MS spectra of three mesophase pitches. There are more lower molecular weight components in FDO-based mesophase pitch, as indicated by the greater abundance of compounds with m/z < 500 in the FDO-NP(0)-MP chromatogram. The average molecular weights of the FDO-NP(0)-MP , FDO-NP(20)-MP and FDO-NP(100)-MP are 840, 1186 and 902, respectively. The result is consistent with the I_{os} parameters from the FT-IR spectral analysis shown in Table 5. The lowest molecular weights of FDO-NP(0)-MP are ascribed to dealkylation reactions which produced large amounts of free radicals which then led to rapid increase of the system viscosity. The higher molecular weight of FDO-NP(20)-MP is a result of the synergistic reactions of FDO and NP. Specifically, the abundant naphthenic structures on the polyaromatic hydrocarbons of NP reduce the dealkylation reaction rate in FDO and then combine with short-chain alkyl groups in FDO to reduce system viscosity and promote polymerization [28]. The higher degree of polymerization results in the coarser optically

anisotropic domain structure of FDO-NP(20)-MP because of the reduced influence of dealkylation reactions, while polymerization reactions play a dominant role in the formation and development of mesophase [31]. Additionally, the lower system viscosity during the co-carbonization of FDO and NP also facilitates molecular stacking to form a more ordered crystal structure which can be expected to be beneficial for improving the grain size in carbon fiber derivatives [14].

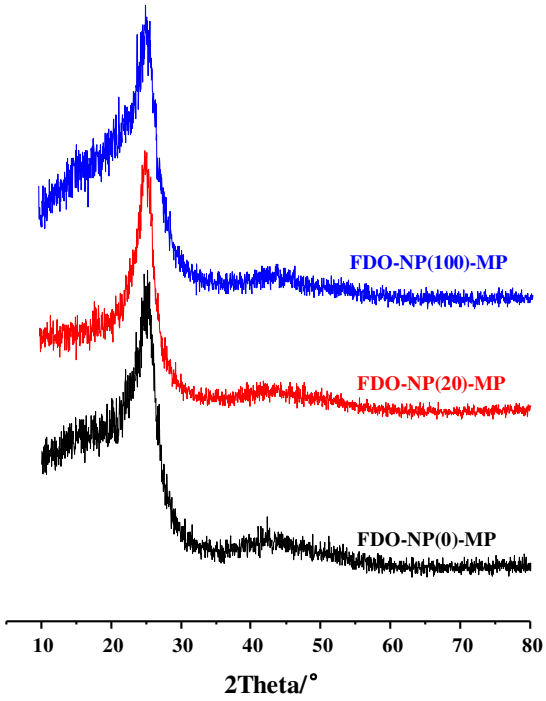

Fig. 9. XRD spectra of selected mesophase pitches

Fig. 9 shows the X-ray diffraction patterns of the same three mesophase pitches and the microcrystalline parameters calculated from the XRD patterns are summarized in Table 10. With the increase of the mass ratio of NP in the feedstocks, the d-spacing of the (002) planes in the mesophase pitches decreases and the stacking heights (L_c) and numbers of carbon layers (N) of the mesophase pitches increase as shown in Table 10. This implies that the crystal structure of FDO-NP(20)-MP is

more ordered than that of FDO-NP(0)-MP. It also indicates that the addition of NP during the co-carbonization of FDO and NP is beneficial for the preparation of mesophase pitch with ordered crystal structure, which is also consistent with the results of optical texture and TOF-MS analyses of the mesophase pitches.

Table 7. Microcrystalline parameters and viscosity of selected mesophase pitches

Sample	d_{002}/nm	L_c/nm	N[g]	Viscosity[h]/Pa·s
FDO-NP(0)-MP	0.352	2.21	7.27	2063
FDO-NP(20)-MP	0.350	2.70	8.71	37
FDO-NP(100)-MP	0.349	2.80	9.03	22

[g] Numbers of layers stacked coherently, $N=L_c/d_{002}+1$,

[h] The viscosity was measured at 330 °C by capillary rheometer

3.4 Carbon fiber prepared from the mesophase pitch

The FDO-derived mesophase pitch is not spinnable because of its high softening point and mosaic-like optical texture. However, pitch fibers are easy to melt-spin from the mesophase pitch FDO-NP(20)-MP. The excellent spinning performance of this pitch is attributed to its good rheological properties and ordered crystal structures. Resulting carbon fibers after graphitization at 3000 °C were labelled as FDO-NP(20)-CFs. Fig.10(a-b) show SEM images of FDO-NP(20)-CFs and commercial carbon fibers, K-1100 [33]. The transverse cross-section of FDO-NP(20)-CFs exhibits a typical radial open wedge texture whereas the K-1100 demonstrates a slightly distorted radial open wedge texture. The mechanical

performance of FDO-NP(20)-CFs, shown in Table 8, is lower than that of the K-1100 reported by the manufacturer[34]. However, the FDO-NP(20)-CFs have higher axial thermal conductivity than that of K-1100, as also shown in Table 8. This is consistent with their larger crystal size (L_a and L_c) compared with that of K-1100. As previously reported, the micro-texture size of carbon fibers largely depends on the molecular stacking height [34] and the spinning viscosity of the mesophase pitch [14, 35]. The large crystal size and high thermal conductivity of FDO-NP(20)-CFs may be attributed to the higher molecular stacking height and lower viscosity of its precursor pitch cf. FDO-NP(0)-MP, as shown in Table 7. The abundant naphthenic structures and short-chain alkyl groups in mesophase pitch prepared via co-carbonization resulted in highly oriented aromatic carbon layers and high layer stacking height for this mesophase pitch, and this also led to it having a relatively low spinning viscosity.

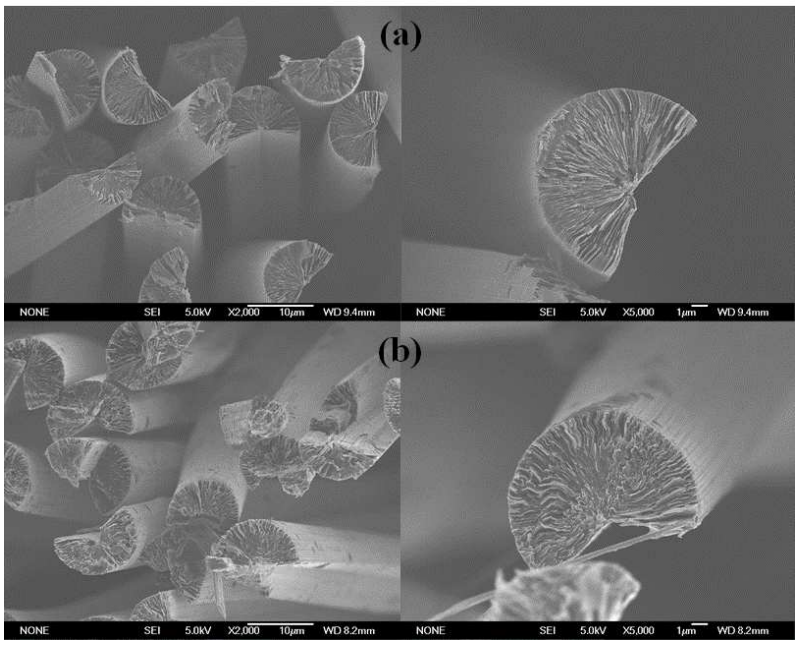

Fig. 10. SEM micrographs of (a) graphitized FDO-NP(20)-CFs and (b) K-1100

Table 8. Properties and crystal parameters of FDO-NP(20)-CFs and K-1100 graphite fibers

Sample	Properties					Crystal parameters		
	Elongation[i] /%	TS[j] /GPa	TM[k] / GPa	P[l] /μΩ·m	TC[m]/ W/(m·K)	d_{002} /nm	L_a[n] /nm	L_c /nm
FDO-NP(20)-CFs	0.45	2.70	673	1.14	1106	0.3364	90.13	39.05
K-1100[φ]	0.30	3.10	931	1.17	1078	0.3366	79.68	38.53

[i] Elongation to failure, [j] Tensile strength, [k] Tensile modulus, [l] Room-temperature axial electrical resistivity, [m] Axial thermal conductivity calculated by the formula: TC=1261/ρ [36].

[n] L_a=0.95/(d_{002}-0.3354) [37].

[φ] Mechanical performance data were reported by the manufacturer

4. Conclusions

Spinnable mesophase pitches with low softening point, good solubility and 100 vol% anisotropic content were synthesized by co-carbonization of FDO and synthetic NP. The solubility and optically anisotropic domain size of the resultant mesophase pitches are improved with the addition of NP into the feedstock. Molecular structure analysis shows that FDO contains both abundant naphthenic structures and short-chain alkyl groups while NP is rich in naphthenic structures with only a few short-chain alkyl groups. The naphthenic structures of the polyaromatic hydrocarbons in NP show higher thermal stability than those in FDO. The synergistic reactions of these naphthenic structures in NP with short-chain alkyl groups in FDO result in the formation of mesophase pitch with larger molecular weight than that of both its components via co-carbonization. The graphitized fibers prepared from FDO-NP(20)-MP show higher thermal conductivity and larger crystal size of than those of K-1100, and this

is ascribed to the more ordered structure and lower spinning viscosity of the synthesized FDO-NP(20)-MP mesophase pitch.

Acknowledgments

This work was sponsored by the National Natural Science Foundation of China (No. U1864207). The authors appreciate the support of Jinzhou Petrochemical Co., China for providing the FDO.

References

[1] Chen, C.; Kennel E. B.; Stiller A. H.; Stansberry P. G.; Zondlo J. W. *Carbon* **2006**, 44 (8), 1535-1543.

[2] Kumar, S.; Srivastava, M. *J. Ind. Eng. Chem.* **2017**, 48, 133-141.

[3] Guo, Y.; Li, Y.; Ran, N.; Gao, F. *J Mater Sci* **2016**, 51 (5), 2558-2564.

[4] Kumar, S.; Srivastava, M. *Fuel* **2016**, 173, 69-78.

[5] Cristadoro, A.; Kulkarni, S. U.; Burgess, W. A.; Eduardo, G. C.; Hans, J. R.; Klaus, R., David, A. B.; Mark, C. T. *Carbon* **2009**, 47 (10), 2358-2370.

[6] Lee, S.; Eom, Y.; Kim, B. J.; Mochida, I.; Yoon, S. H.; Kim, B. C. *Carbon* **2015**, 81 (1), 694-701.

[7] Yamada, Y.; Honda, H., Inoue, T. Japan Patent 5818421, 1983.

[8] Abrahamson, J. P.; Wincek, R. T.; Eser, S. *Energy & Fuels* **2016**, 30 (10).

[9] Yang, D. P.; Korai, Y.; Mochida, I. *J Mater Sci* **1986**, 21 (2), 424-428.

[10] Yang, D. P.; Mochida, I. *Carbon* **1989**, 27 (6), 925-929.

[11] Singer, L. S.; Riffle, D. M.; Cherry, A. R. *Carbon* **1987**, 25 (2), 249-257.

[12] Korai, Y. Mochida, I. *Carbon* **1985**, 23 (1), 97-103.

[13] Li, W. D.; Chen, Y.; Zhang, L. Z.; Xu, Z. M.; Sun, X. W.; Zhao, S. Q.; Xu, C. M. *Energy & Fuels* **2016**, 30 (12).

[14] Mochida, I.; Shimizu, K.; Korai, Y.; Sakai, Y.; Fujiyama, S.; Toshima, H.; Takashi, H. *Carbon* **1992**, 30 (1), 55-61.

[15] Korai, Y.; Nakamura, M.; Mochida, I.; Sakai, Y.; Fujiyama, S. *Carbon* **1991**, 29 (4-5), 561-567.

[16] Yoon, S. H.; Korai, Y.; Mochida, I. *Carbon* **1993**, 31 (6), 849-856.

[17] Mochida, I.; Shimizu, K.; Korai, Y.; Otsuka, H.; Sakai, Y.; Fujiyama, S. *Carbon* **1990**, 28 (2-3), 311-319.

[18] Li, M.; Liu, D.; Lou, B.; Hou, X. L.; Chen, P. *Energy & Fuels* **2016**, 30 (10).

[19] Yang, J.X.; Nakabayashi, K.; Miyawaki, J.; Yoon, S. H. *Carbon* **2016**; 106, 28-36.

[20] Eser, S.; Wang, G.H. *Energy Fuels* **2007**, 21 (6), 3573-3582.

[21] Siddiqui, M.N.; Ali, M.F.; Shirokoff, J. *Fuel* **2002**, 81 (1), 51-58.

[22] Feret, F.R. *Analyst* **1998**, 123 (4), 595-600.

[23] Machnikowski, J.; Kaczmarska, H.; Leszczyńska, A.; Rutkowskti, P.; Díezb, M. A.; Álvarez, R.; Garcíab, R. *Fuel Process. Technol.* **2001**, 69 (2), 107-126.

[24] Diaz, C.; Blanco, C.G. *Energy & Fuels* **2003**, 17 (4), 907-913.

[25] Gargiulo, V.; Apicella, B.; Alfè, M.; Russo, C.; Stanzione, F.; Tregrossi, A.; Amoresano, A.; Millan, M.; Ciajolo, A. *Energy & Fuels* **2015**, 29 (9).

[26] Korai, Y.; Mochida, I. *Carbon* **1992**, 30 (7), 1019-1024.

[27] Li, M.; Liu, D.; Men, Z.; Lou, B.; Yu, S. T.; Ding, J.W.; Cui, W. L. *Fuel* **2018**, 222, 617-626.

[28] Li, X.; Qing, C.; Yang, X. *Petrochemical Technology* **2007**, 36(11), 1104-1109.

[29] Russo, C.; Stanzione, F.; Tregrossi, A.; Ciajolo, A. *Carbon* **2014**, 74 (8), 127-138.

[30] Li, M.; Liu, D.; Lou, B.; Zhang, Y. D. *Rsc Advances* **2018**, 8 (7), 3750-3759.

[31] Greinke, R. A. *Carbon* **1990**, 28 (5), 701-706.

[32] Emmerich, F. G. *Carbon* **2014**, 79 (1), 274-293.

[33] Minus, M.; Kumar, S. *JOM* **2005**, 57 (2), 52-58.

[34] Yang, H.; Yoon, S. H.; Korai, Y.; Mochida, I.; Katou, O. *Carbon* **2003**, 41 (3), 397-403.

[35] Yoon, S.H.; Korai, Y.; Mochida, I.; Kato, I. *Carbon* **1994**, 32 (2), 273-280.

[36] Zhang, X.; Fujiwara, S.; Fujii, M. *International Journal of Thermo- physics* **2000**, 21 (4), 965-980.

[37] Schenk, A., Winter, B.; Lutterloh, C.; Biener, J.; Schubert, U. A.; Küppers, J. *Journal of Nuclear Materials* **1995**, 220-222, 767-770.